

A NEW APPROACH TO SPINDLE RADIAL ERROR EVALUATION USING A MACHINE VISION SYSTEM

C. Kavitha, S. Denis Ashok

VIT University, School of Mechanical Engineering, Vellore-632014, Tamil Nadu, India
(kavitha.c@vit.ac.in, ✉ denisashok@vit.ac.in, +91 94 4486 8585)

Abstract

The spindle rotational accuracy is one of the important issues in a machine tool which affects the surface topography and dimensional accuracy of a workpiece. This paper presents a machine-vision-based approach to radial error measurement of a lathe spindle using a CMOS camera and a PC-based image processing system. In the present work, a precisely machined cylindrical master is mounted on the spindle as a datum surface and variations of its position are captured using the camera for evaluating runout of the spindle. The *Circular Hough Transform* (CHT) is used to detect variations of the centre position of the master cylinder during spindle rotation at subpixel level from a sequence of images. Radial error values of the spindle are evaluated using the Fourier series analysis of the centre position of the master cylinder calculated with the least squares curve fitting technique. The experiments have been carried out on a lathe at different operating speeds and the spindle radial error estimation results are presented. The proposed method provides a simpler approach to on-machine estimation of the spindle radial error in machine tools.

Keywords: machine vision, circular hough transform, Fourier series, runout, spindle radial error.

© 2017 Polish Academy of Sciences. All rights reserved

1. Introduction

A spindle is one of the key functional elements in a typical machine tool which provides a rotation to a work piece or tool. The rotational accuracy of the spindle is an important issue in production of accurate and precise components. Runout of the spindle is caused due to an installation error resulting in a misalignment of its rotational axis with either a tool or workpiece. It leads to varying a chip load on the cutting tool and machining inaccuracies related to tool positioning, causing the surface location error [1]. In early years, spindle runout tests were performed for assessing the spindle accuracy by installing a master in the spindle and measuring the *total indicated runout* (TIR) using a mechanical displacement indicator. However, the total indicated runout is not the true indicator of spindle accuracy as it is the superposition of the form error of the measured surface and the error of the spindle motion. Capacitive-sensor-based measurement techniques have been widely applied to meet the high accuracy requirement of metrology applications. A capacitive-sensor-based surface parameter evaluation method and its application to the surface finish measurement system is presented in [2]. The accuracy of spindle error measurement using capacitive sensors is affected by inherent error sources, such as a sensor offset, a thermal drift of spindle, the centring error, and the form error of the target surface installed in the spindle [3]. These methods require a measurement setup consisting of multiple numbers of sensors and instrumentations such as an angular index table, fixtures, *etc.* Hence, there is a need for developing a suitable measurement and evaluation technique of spindle runout for understanding the machining performance of the machine tool.

Laser-based optical measurement techniques have been developed by the researchers for evaluation of the spindle accuracy in machine tools. An optical measurement system consisting of a laser diode and position-sensitive detectors is used for measuring the spindle error during motions in high-speed conditions [4]. A laser interferometer is used for measuring the spindle rotation errors such as the radial motion error and axial motion error in a lathe [5]. An optical measurement system consisting of a rod lens, a ball lens, a laser beam, and a photodiode is developed for measuring rotational errors of a micro-spindle [6]. Fujimaki and Mitsui developed an optical measurement system consisting of a laser diode, a quadrant photodetector and a beam splitter for measuring the spindle radial runout of a miniaturized machine tool [7]. Though the laser-based measurement techniques have a longer working distance, they require extensive experimental arrangements and more setup time for aligning the laser path with the optics. With the recent advancements in computing and imaging systems, machine vision systems have been widely applied for different industrial inspection applications. A vision-based measurement technique using a CCD camera and a lens arrangement was proposed for measuring the radial errors of a cutting tool [8]. A change in position of the cutting tool is measured using a thresholding-based edge detection method.

It was noticed that the accuracy of spindle error measurement using a machine vision system was limited by the edge detection algorithms and lighting conditions. Hence, there is a need for developing suitable image processing algorithms to improve the accuracy of edge detection for estimation of the spindle runout using a machine vision system. Also, existing methods of spindle runout estimation are not suitable for on-machine inspection due to the requirements of multiple sensors and measurement setups for removing the contribution of the form error of the master cylinder. In order to overcome this difficulty, this work focuses on developing an image processing method suitable for online estimation of spindle runout in a lathe using a *Circular Hough Transform* (CHT)-based subpixel circle detection method. In the proposed method, a circle is detected in the images for measuring the radial error of the spindle; hence, it does not take into account the contribution of the form error of the master cylinder. The experimental results of the proposed method for evaluating the spindle radial error of a lathe are presented and discussed in this paper.

2. Development of machine vision system for spindle runout estimation

In the present work, a machine vision system consisting of a CMOS camera, a frame grabber and a PC image acquisition system is developed for estimation of the spindle radial error in a lathe. A precisely machined master cylinder is mounted on the lathe spindle and used as a target to measure the runout of the spindle. It is important to capture high quality images in the uniformly illuminated area of interest for machine-vision-based inspection applications. In the present work, a front lighting system with a ring arrangement of red LEDs is used to illuminate the circular face of the master cylinder. This lighting arrangement provides a shadow-free illumination and the red LED light is intensive enough to block the ambient light on the master cylinder. A lighting intensity is manually adjusted and controlled to provide uniform illumination on the circular face of the master cylinder using a regulated power supply. Details of the experimental arrangement for the spindle radial error estimation in a lathe are explained in this Section.

2.1. Experimental arrangement for image acquisition

The machine vision system used for measurement of the spindle radial error consists of a monochrome CMOS camera (AVT Marlin F-131b), a frame grabber (IEEE-1394A) and a PC with the LABVIEW software (Version.8.0) for storing images of the spindle as shown

in Fig. 1a. General specifications of the CMOS camera used in the present work are listed in Table 1.

Table. 1 Specifications of the camera used for measurement of the spindle radial error.

Items	Description
Camera Model	AVT Marlin F-131b
Image device	Type 2/3 (diag. 11 mm) global shutter CMOS sensor
Effective picture elements	1280 (H) x 1024 (V)
Cell size	6.7 μm x 6.7 μm
Resolution depth	8 bit; 10 bit (ADC)
Lens mount	C-Mount
Digital interface	IEEE 1394 IIDC v. 1.3
Power consumption	Less than 3 watt (@ 12 V DC)
Dimensions	72 mm x 44 mm x 29 mm (L x W x H); w/o tripod and lens

In order to measure the radial error of the spindle, a cylindrical master cylinder of 13 mm diameter is mounted on the lathe spindle and the CMOS camera is placed firmly on the tool post of the lathe to focus on the circular face of master cylinder. A distance between the camera and the master cylinder was measured using a standard scale and it was found to be 40 cm. The horizontal and vertical tilts of the camera in relation to the base of the tool post was checked using a spirit level, as shown in Fig. 1c. Screws in the tool post were manually adjusted until the bubble in the spirit level remained in the centre position, thus eliminating the misalignment of the camera.

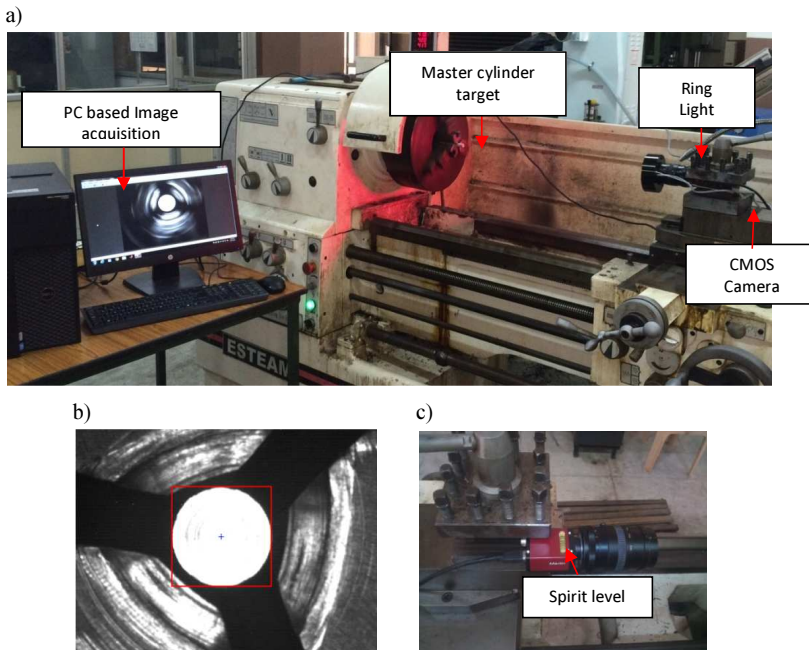


Fig. 1. The experimental arrangement for spindle radial error measurement using the vision system in a lathe. Important elements of the machine vision system for spindle radial error measurement (a); an image of the master cylinder (b); verification of alignment of the camera using a spirit level.

Further, the effect of misalignment of camera was analysed by calculating an aspect ratio of the circular face of the master cylinder in the image. The aspect ratio is defined as a ratio of the width of minimum enclosing rectangle of an object and the length of that object [9], as given below:

$$A = \frac{W}{L}. \quad (1)$$

Figure 1b shows the minimum enclosing rectangle for the master cylinder and the value of aspect ratio is calculated to be 1, which ensures the proper alignment of the camera. After verifying the alignment of the camera, a sequence of images of the master cylinder are captured with a resolution of 800 pixels x 600 pixels for different spindle speeds and stored using the LABVIEW Image acquisition software in the PC. As the maximum frame rate of the camera is 30 fps, the spindle radial error measurements were carried out at lower spindle speeds. Fig. 2 shows sample images acquired for a spindle speed of 25 rpm.

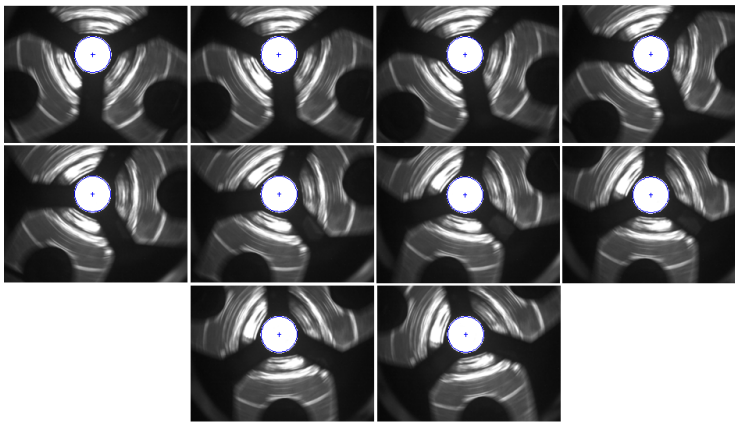


Fig. 2. A sequence of master cylinder images acquired at a spindle speed of 25 rpm.

Evaluation of radial error of the spindle using the digital images requires a suitable edge detection algorithm for detecting the change in position of the master cylinder, and calibration of the camera for specifying the measured values in the real world units.

2.2. Camera calibration

The camera calibration is an essential step in machine vision inspection applications to obtain metric information from the images. In this work, the camera calibration is carried out using a standard slip gauge at a known distance [10]. Back lighting is used for acquiring the exact boundary of the slip gauge, as shown in Fig. 3. The number of pixels in x and y directions was counted in the image of the slip gauge and the scale factor for converting the pixel values into the real world units is determined using the dimension of the slip gauge in x , y directions, as given below:

Figure 3a shows the arrangement for acquiring the image of the slip gauge using a backlighting system. In this work, a slip gauge of dimension 30 mm x 4 mm is used, as shown in Fig. 3b; the numbers of pixels in x , y directions are found to be 361 pixels x 48 pixels, respectively. Hence, the conversion factor for obtaining measurements in the real world unit is calculated as 0.083 mm/pixel.

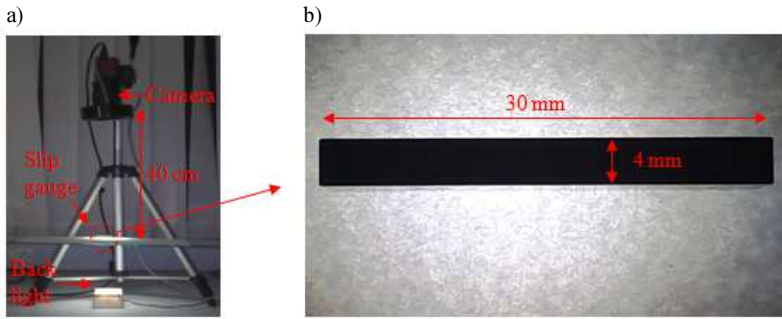


Fig. 3. Calibration of the camera using a slip gauge.

$$P_x = \frac{\text{Dimension of blocks in x direction}}{\text{Number of pixels in x direction}}, \quad (2)$$

$$P_y = \frac{\text{Dimension of blocks in y direction}}{\text{Number of pixels in y direction}}. \quad (3)$$

2.3. Edge detection using canny edge detection method

The canny edge detection is a popular method for identifying the edge pixels of objects in the acquired images [11]. Commonly, edges in the digital images are detected based on significant changes in the grey level of pixels using first derivatives in respective directions. In the canny edge detection method, a magnitude of gradient and a direction of pixels are calculated for detecting changes in the grey level of pixels. The magnitude and direction of a gradient G are given by:

$$|\nabla I| = G = \sqrt{G_x^2 + G_y^2}, \quad (4)$$

$$\theta = \text{atan}(G_x, G_y), \quad (5)$$

where G_x , G_y are partial derivatives of the image I along x and y , respectively. The pixels with the gradient value above a threshold have been grouped and identified as edge pixels, and the remaining gradients below the threshold are lumped into the background with no information. Fig. 4 shows the results of edge detection using the canny edge detection method for the acquired image.

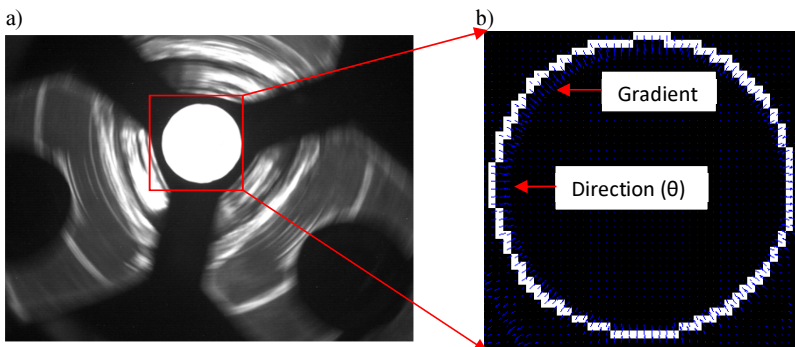


Fig. 4. Application of the canny edge detection for identifying edge pixels. A grey scale image of the master cylinder (a); detected edge pixels using gradient (b).

In the presence of noise, the edge pixels identified by the canny edge detecting algorithm using gradients cannot define the boundary of the master cylinder accurately [10]. Hence, in the present work, the CHT is applied to the images for the accurate edge detection of the master cylinder and for evaluating the radial error of the spindle.

3. Circle detection using Circular Hough Transform

In the present work, the Circular Hough Transform is applied to the edge detection of master cylinder at a subpixel level to find the radial error of the spindle. The major advantage of this transform is its robustness towards irregularities in detected objects and disturbances like noise under varying illumination [12]. In the proposed method, the contribution of the form error of master cylinder is not taken into account, assuming the shape of the master cylinder to be a circle, for improving the accuracy of spindle radial error evaluation. The CHT is used to determine the circle parameters when the edge pixels are known. The steps involved in the CHT for the spindle runout estimation are shown in Fig. 5 and are explained in the subsequent Sections:

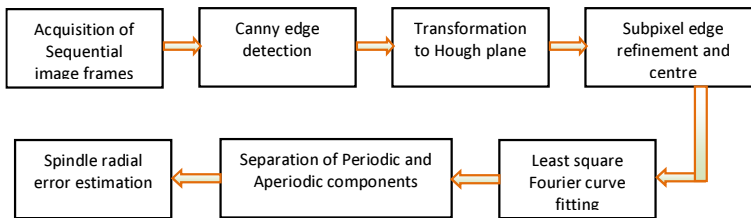


Fig. 5. The proposed method for spindle radial error evaluation.

3.1. Transformation of edge pixels for circle detection in Hough plane

The key idea of the CHT is computation of the circle parameters [13], such as a circle centre and its radius (X_c, Y_c, R) in images by mapping the edge pixels in the image space onto the parameter space or the Hough space. The characteristic equation of a circle with a radius R and centre (X_c, Y_c) is given below:

$$(x - X_c)^2 + (y - Y_c)^2 = R^2. \tag{6}$$

Here, the unknown parameters are the centre point's coordinates (X_c, Y_c) and the radius R . (x, y) is the edge location of a circle obtained by finding the maximum gradient above a predefined threshold value. Fig. 6 shows the transformation of an edge point in the image plane as the centre point of a circle with an unknown arbitrary radius R in the Hough space.

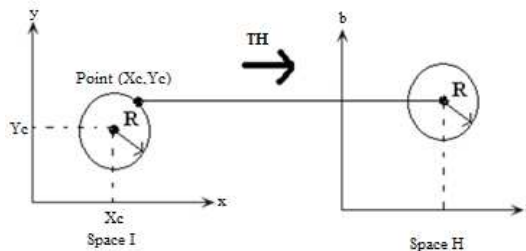


Fig. 6. Transformation of an edge point of a circle [14].

Each edge pixel of the image plane (x, y) is transformed onto the centre coordinates of a circle and the circle is drawn with the fixed radius (R) in the Hough plane using the gradient direction of the edge pixels, as given in [14]:

$$X_c = x - R * \cos(\theta), \tag{7}$$

$$Y_c = y - R * \sin(\theta), \tag{8}$$

where (x, y) are the locations of edge pixels obtained from the gradient and θ are the directions of the gradients of edge pixels. When this transformation is applied to all the edge pixels, it corresponds to the number of circles with a given arbitrary radius R in the Hough plane, as shown in Fig. 7.

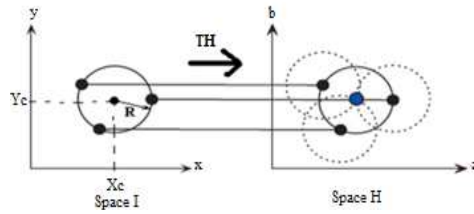


Fig. 7. Intersection of circles and centre estimation [14].

It is found that the edge pixels in the image plane form full circles with a desired radius R in the Hough plane, where their intersection is identified as the centre point (X_c, Y_c) of the detected circle in the image plane.

3.2. Discretization of circle parameters and accumulator array computation

The most important parameter while detecting a circle is its radius. It determines the size of circles plotted in the parameter space. In order to find the unknown radius of the circle in the image plane, a range of values (R_{max}, R_{min}) is chosen arbitrarily using the following constraint:

$$R = R_{min} < (x^2 + y^2) < R_{max}^2. \tag{9}$$

An accumulator array is initialized to count and store values of centre coordinates of the circles for all edge pixels and a given value of radius in the range of values (R_{max}, R_{min}) , as below:

$$X_c = x - [R_{min}:R_{max}] * \cos(\theta), \tag{10}$$

$$Y_c = y - [R_{min}:R_{max}] * \sin(\theta). \tag{11}$$

For a given edge point in the circle of the image plane, if the circle is drawn with the desired radius in the Hough plane, the accumulator stores corresponding coordinates of the circle centre and radius. This count is increased for all the edge pixels in the accumulator array every time the circle is drawn with the desired radius of the circle. The accumulator array which provides the maximum count for coordinates of the circle centre and its radius is identified by a search method to find the circle centre and radius in the image plane at a subpixel level. The location of circle centre defines the location of datum axis of the master cylinder and detecting the edges of the master cylinder in the image plane.

3.3. Fourier series analysis of circle centre coordinates

The estimated circle centres contain the contribution of the centring error of the spindle which is periodic in nature for every revolution of the spindle [3]. In the present work,

the periodic components of the circle centre coordinates are extracted using the Fourier curve fitting method in the time domain. The proposed mathematical model for interpreting the time sampled centre coordinates of the master cylinder is given by the following Fourier series formula:

$$X_{ci} = r_0 + \sum_{h=1}^H (a_h \cos(w * h * t_i) + b_h \sin(w * h * t_i)), \quad (12)$$

where $i = 1, 2, 3, \dots, m$; and $m =$ the number of samples of centre coordinates considered for analysis; H is the number of harmonics; $h = 1, 2, \dots, H$; and (a_h, b_h) are Fourier coefficients which describe the repeatable components of the measurement data, such as the centring error, the form error of the target object, and the synchronous radial error of the spindle. X_{ci} are the centre coordinates of master cylinder along x-axis, $X_{ci} = [X_{c1}, X_{c2}, \dots, X_{cm}]^T$. The sampling time is calculated based on the frame rate of image acquisition and it is given by $t_i = [t_1, t_2, \dots, t_m]^T$.

In the present work, the time taken for acquisition of an image frame is 1/30 of a second.

The time taken to complete one revolution is calculated from the time sampled circle centre data and it is denoted as T :

$$w = 2 * \frac{\pi}{T}. \quad (13)$$

A linear least square method is used to estimate the unknown Fourier coefficients by minimizing the sum of squares of deviations of measured data [15]:

$$\begin{bmatrix} X_{c1}' \\ X_{c2}' \\ X_{c3}' \\ \vdots \\ X_{cm}' \end{bmatrix} = \begin{bmatrix} 1 & \cos(w * t_1) & \sin(w * t_1) & \cdot & \cos(w * H * t_1) & \sin(w * H * t_1) \\ 1 & \cos(w * t_2) & \sin(w * t_2) & \cdot & \cos(w * H * t_2) & \sin(w * H * t_2) \\ 1 & \cos(w * t_3) & \sin(w * t_3) & \cdot & \cos(w * H * t_3) & \sin(w * H * t_3) \\ \vdots & \vdots & \vdots & \vdots & \vdots & \vdots \\ 1 & \cos(w * t_m) & \sin(w * t_m) & \cdot & \cos(w * H * t_m) & \sin(w * H * t_m) \end{bmatrix} \begin{bmatrix} r_0 \\ a_1 \\ b_1 \\ \vdots \\ a_H \\ b_H \end{bmatrix}. \quad (14)$$

The above equation can be simplified to:

$$D = \begin{bmatrix} 1 & \cos(w * t_1) & \sin(w * t_1) & \cdot & \cos(w * H * t_1) & \sin(w * H * t_1) \\ 1 & \cos(w * t_2) & \sin(w * t_2) & \cdot & \cos(w * H * t_2) & \sin(w * H * t_2) \\ 1 & \cos(w * t_3) & \sin(w * t_3) & \cdot & \cos(w * H * t_3) & \sin(w * H * t_3) \\ \vdots & \vdots & \vdots & \vdots & \vdots & \vdots \\ 1 & \cos(w * t_m) & \sin(w * t_m) & \cdot & \cos(w * H * t_m) & \sin(w * H * t_m) \end{bmatrix}$$

$$x = [r_0, a_1, b_1, \dots, a_H, b_H]^T$$

Therefore:

$$X_c' = Dx. \quad (15)$$

The Equation (14) leads to an over-determined system of simultaneous linear equations (*i.e.* $m > 2H + 1$). In this case, there exist residuals between the measurement data and the fitted curve, given by:

$$e_i = (X_{ci}' - Dx). \quad (16)$$

Assuming the residuals follow a normal probability distribution, the solution for the unknown model parameters can be obtained by minimizing the sum of squared residuals using a linear least square approach, as given by (17):

$$\hat{x} = [(D^T D)^{-1} D^T] X_{ci}' = [\hat{r}_0, \hat{a}_1, \hat{b}_1, \dots, \hat{a}_H, \hat{b}_H]. \quad (17)$$

Here, H represents the number of harmonics considered for evaluating the radial error of the spindle. The centring error of the master cylinder represents the first harmonic ($h = 1$) and it can be removed from the measurement data, which is given as:

$$\hat{X}_{c-cen} = \hat{a}_1 \cos(w * t_i) + \hat{b}_1 \sin(w * t_i). \quad (18)$$

The remaining harmonic components ($H > 2$) contribute to the synchronous radial error of the spindle and they can be extracted using the following formula:

$$\hat{X}_{c_syn} = \sum_{h=2}^H \hat{a}_h \cos(w * H * t_i) + \hat{b}_h \sin(w * H * t_i). \quad (19)$$

This value is further analysed in a polar plot for evaluating the synchronous radial error of the spindle. The residuals of the measurement data for the fitted curve represent the asynchronous radial error of the spindle which is calculated using (16). It is further analysed in the polar plot for evaluating the asynchronous radial error of the spindle.

3.4. Estimation of radial error of spindle in polar plot

A polar plot is commonly used for displaying the spindle error evaluation results with a base circle [3] and it requires the angular position of the spindle. The angular position of the spindle for a given time t_i can be calculated using the following formula:

$$\theta_i = \omega * t_i. \quad (20)$$

Here, the value of w is calculated using (13). The above equation is useful in plotting the synchronous and asynchronous radial error values of the spindle in a polar plot.

In accordance with the *ANSI/ASME B89.3M* standard, the least squares circle centre is calculated from the periodic components used for evaluating the synchronous radial error of the spindle after removing the contribution of the centring error of the spindle[16]. The asynchronous radial error is calculated from the aperiodic components of circle centre as the maximum deviation for a given spindle speed.

4. Results and discussions

The CHT-based circle detection approach is applied to a sequence images for estimation of the master cylinder centre. The results for estimated values of circle centres are presented for the sequence of images obtained for a spindle speed of 25 rpm. Further, the centre coordinates of the master cylinder are analysed using the least squares curve fitting technique to separate the contribution of the centring error of the master cylinder and the synchronous and asynchronous errors of the spindle. As the least squares curve fitting method provides an approximation of the ideal curve assuming the residuals follow a normal distribution, the error of the estimation obtained by the least squares curve fitting method is evaluated using the simulated circle centre data. The simulation and experimental results of the least squares curve fitting method are presented. Further, the spindle radial error values are evaluated for different spindle speeds and the results are presented.

4.1. Estimation circle centre using CHT

In order to reduce the computation time and complexity of the transform, a range of radii of the master cylinder has been fixed manually. Fig. 8 shows the accumulator array computation results in the Hough space in 2D and 3D views for different ranges of radii. When a broader radius range of 15 pixels ($R_{max} - R_{min} = 15$) is fixed, the maximum votes for the centre of the circle accumulate at (386, 214), as shown in Fig. 8a.

To further reduce the computation time, a finer range of 6 pixels is fixed and the computed accumulator array is shown in Fig. 8b. In this case, the circle centre estimation is also found to be (386,214). This proves the robustness of the CHT method in detecting the circle centre coordinates in the image plane for a change of the search radius in the image plane. The estimated centre coordinates of circle in the Hough plane are located in the image plane

and they are used in identifying the edge of the master cylinder at a subpixel level, as shown in Fig. 9. The subpixel level identification of circle edge is shown in Fig. 9b as compared with the pixel level edge detection using a canny edge detector. This result confirms an improved edge detection at a subpixel level for the master cylinder in given images as compared with the conventional canny edge detection method. The estimated values of circle centre require further analysis in the time domain for evaluation of the radial error of the spindle.

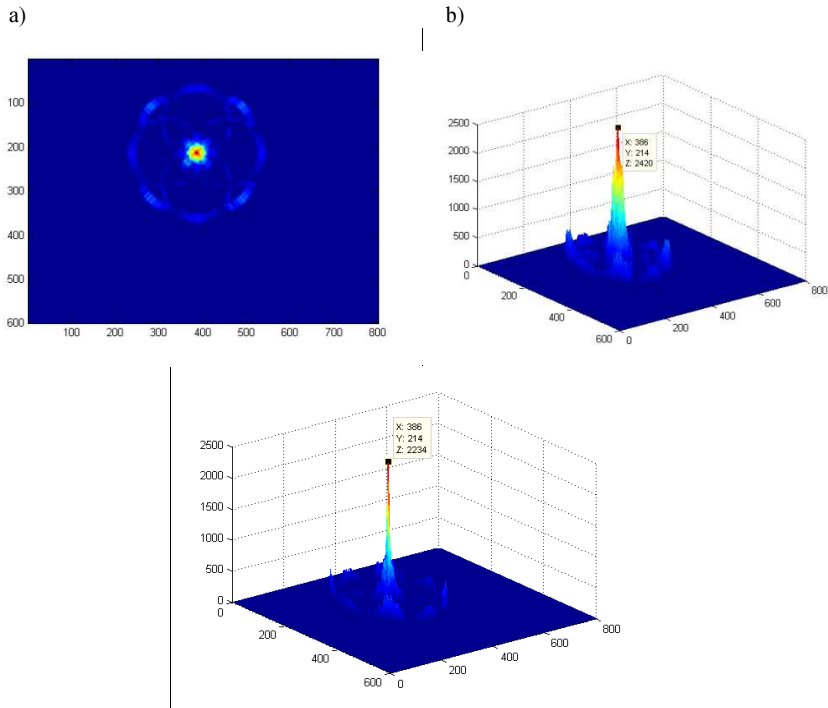


Fig. 8. 2D and 3D views of the accumulator array for the computation of circle centre. A larger width of radius range (15 pixels) (a); a smaller width of radius range (6 pixels) (b).

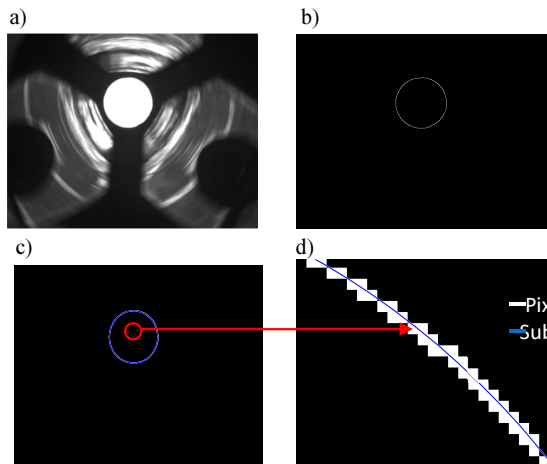


Fig. 9. Pixel and Subpixel level edge refinement. Input image (a); canny edge (b); Hough circle fitting (c); subpixel edge (d).

4.2. Time domain analysis of circle centre data

The CHT is applied and estimated The values of circle centre estimated with applying CHT to a sequence of images for different spindle speeds are shown in Fig. 10. They indicate that a change in position of the master cylinder in the Cartesian plane is found to remain within a range of 212.5–214.5 pixels in Y direction and 385–387.5 pixels in X direction.

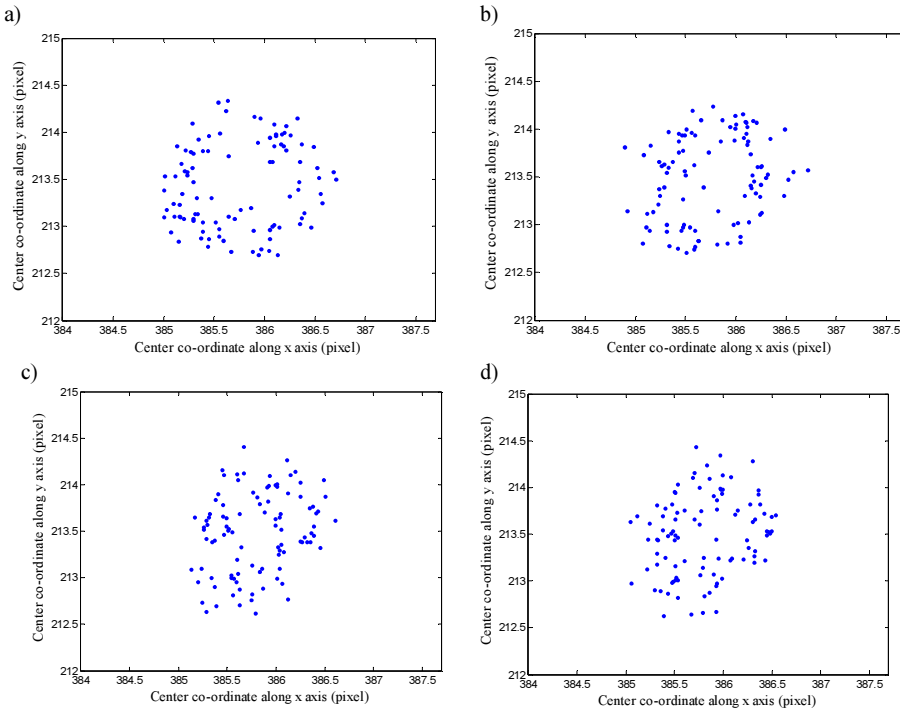


Fig. 10. The values of circle centre coordinates estimated using CHT. 25 rpm (a); 50 rpm (b); 75 rpm (c); 100 rpm (d).

Evaluation of radial error of the spindle requires further analysis of the circle centre values in the time domain. As the frame rate of camera is 30 frames/sec, a time stamp is attached to the circle centre coordinates for a given image frame. Table 2 shows samples of the circle centre coordinates and the sampling time for a spindle speed of 25 rpm.

Table 2. Samples of the circle centre coordinates estimated using the CHT method.

Frame number	Time (Sec)	Coordinates of circle centre (pixels)	
		X_c	Y_c
Frame 1	0.00	386.2496	213.3237
Frame 2	1/30	385.7641	213.182
Frame 3	2/30	385.9357	212.6999
Frame 4	3/30	386.0461	212.8709
Frame 5	4/30	386.0446	212.7411
Frame 6	5/30	385.5476	212.9786
Frame 7	6/30	385.4458	212.8686
Frame 8	7/30	385.5866	212.8536
Frame 9	8/30	385.3831	212.9457
Frame 10	9/30	385.2956	213.0832

The mean value of the circle centre along X direction is calculated and subtracted from each centre coordinate to provide a reference in the time domain. Further, the units of the centre coordinates in the images are converted from pixels to microns using a calibration value of 83 micron/pixel. Fig. 11 shows samples of corrected and calibrated mean values of the circle centre for a spindle speed of 25 rpm.

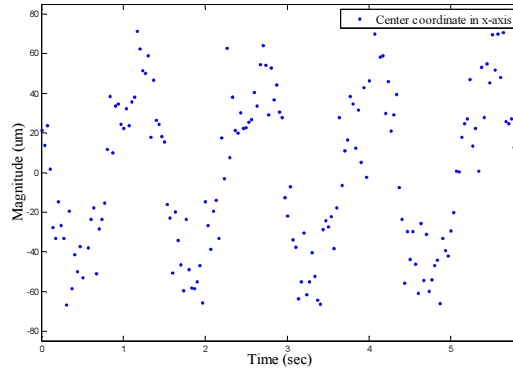


Fig. 11. The corrected and calibrated mean coordinates of circle centre of the master cylinder for a spindle speed of 25 rpm.

A periodically varying sinusoidal trend is observed in the circle centre data in the time domain and it is due to the combined contribution of centring of master cylinder and errors in the axis of rotation of the spindle. The centring error of the master cylinder is considered as a systematic error since it is due to inaccurate mounting of the master cylinder in the spindle [3]. Hence, to evaluate the radial error of the spindle, its contribution needs to be removed. In the present work, to remove the contribution of centring error of the master cylinder, the Fourier curve fitting method is applied to the circle centre data.

4.3. Simulation of circle centre data and application of least squares curve fitting method

A Fourier harmonic series given by the equation (12) is used for generating the periodic components of circle centre data for typical values of model coefficients. Table 3 shows the assumed model coefficients applied to characterizing the periodic components of circle centre data using the first 5 harmonics. Here, the number of harmonics is limited to 5 and a magnitude of the first harmonic is assumed to be higher following the sinusoidal trend in the experimental data and it contributes the centring error of the master cylinder. Magnitudes of other harmonics ($H > 2$) are assumed based on typical values obtained in the experimental data. Further, the asynchronous components of circle centre data are assumed to follow a normal probability distribution with a given standard deviation of 0.5 pixels. The synchronous and asynchronous values of circle centre data are combined to provide the simulated circle centre data.

The least squares curve fitting method is applied to the simulated circle centre data to decompose the periodic and aperiodic components. Fig. 12 shows the curve fitted to the simulated data and following the general sinusoidal trend.

The values of harmonic components estimated using the least square curve fitting method are shown in Table 3. It can be seen that deviations between the estimated and simulated values are found to be less than 2.47%. This proves the effectiveness of the least squares curve fitting method for analysing the circle centre data.

Table 3. Comparison between the simulated and estimated values of model coefficients using the curve fitting method.

Model Coefficients	Simulated values	Estimated values	Error (%)
a_1	5.5729	5.635	1.102
b_1	47.3218	47.32	0.0038
a_2	4.1323	4.115	0.4204
b_2	2.991	2.989	0.0669
a_3	4.0132	3.965	1.2156
b_3	2.8978	2.94	1.4354
a_4	1.0267	0.9513	7.926
b_4	3.5621	3.697	3.6489
a_5	2.0014	2.003	0.0799
b_5	1.0745	1.065	0.892
r_0	0.0405	0.04121	1.7229

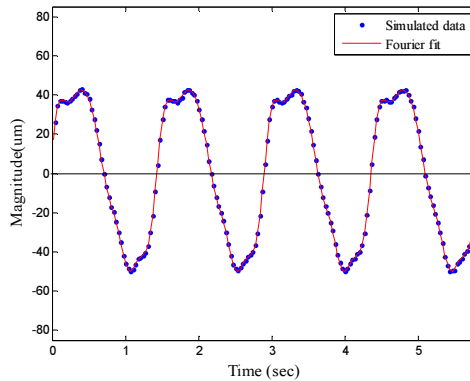


Fig. 12. Application of the least squares curve fitting method for the simulated circle centre data.

4.4. Experimental results of least squares curve fitting method

In order to separate the contribution of the centring error and to evaluate the radial error of the spindle, the coordinates of the circle centre in X direction are further analysed in the time domain using the least squares curve fitting method. The estimated coordinates of circle centre are plotted in the time domain based on a frame rate of image acquisition.

Figure 12 shows the corrected and calibrated mean coordinates of circle centre of the master cylinder and they exhibit a sinusoidal trend which is due to the contribution of the centring error of the master cylinder. In order to remove this contribution and extract the radial error values of the spindle, a least square curve fitting algorithm is applied to circle centre data. Here, a harmonic cut-off value is selected as 15. It can be seen that the fitted curve closely follows the periodic trend of the circle centre data, as shown in Fig.13a. It is also noticed that the periodic trend is repetitive for each revolution of the spindle and the time taken for completion of one revolution is also computed using the periodic trend. The total indicated runout of the spindle is calculated as 142 microns. As shown in Fig. 13b, the residuals show random variations as the periodic components are extracted by the Fourier curve, and they represent the contribution of the asynchronous radial error of the spindle [17].

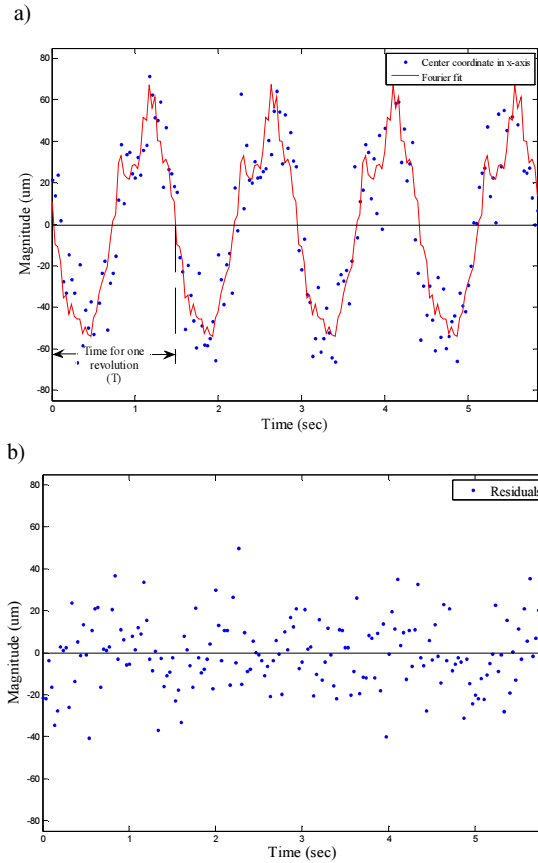


Fig. 13. Fourier series analysis of the circle centre data in X direction. Extraction of periodic components using the least squares fitting of the Fourier curve (a); residuals (b).

The Fourier coefficients estimated by using the least squares curve fitting method is shown in Table 4 for the first five harmonic components. It can be noticed that the first harmonic components are dominant and they represent the contribution of the centering error of the master cylinder. Magnitudes of other harmonic components are found to be less than the first harmonic component one and they represent the combined contribution of the synchronous radial error of the spindle which is due to imperfections in the bearing surface of the spindle.

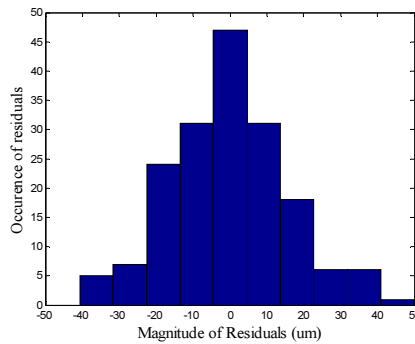


Fig. 14. A histogram of residuals.

Table 4. The values of model parameters of the Fourier curve estimated using the least square method.

Model Coefficients	Estimated values of model coefficients using the proposed method
a_1	32.3702
b_1	-39.4984
a_2	8.4089
b_2	1.5164
a_3	6.7610
b_3	-3.7970
a_4	-2.1307
b_4	-2.5259
a_5	-2.8483
b_5	2.2809
r_0	0.0512

The residuals of the fitted curve from the circle centre data are analysed in a histogram to understand the nature of variation and they are showed in Fig. 14. It can be noticed that most of the residuals are centred around the zero mean which indicates that the distribution is represented by a bell curve. Also, these results validate the assumption about the residuals which follow a normal distribution for the least squares fitting of the Fourier curve.

4.5. Evaluation of spindle radial error

In the present work, a basic circle radius of 5 units is used for displaying the separated components of circle centre data. It is shown in Fig. 15. These plots are obtained for the estimated angular position of the spindle using (20). It can be seen from Fig. 15a that the polar profile of the circle centre data deviates from the base circle, which is due to the contribution of the centring error of the master cylinder. The contribution of the centring error of the master cylinder is separated by using the first harmonic component of the fitted Fourier curve [18] using (18); it is shown in Fig. 15b. It indicates a clear deviation from the base circle and the polar chart centre, which is due to a misalignment of the master cylinder in the axis of rotation of the spindle.

The periodic components of the circle centre data after separation of the centring error is calculated using (19); it is given in Fig. 15c. As the synchronous components of radial error are periodic and repeatable, a magnitude of variation is significantly smaller for every revolution and its value obtained by using the least squares circle centre is 10.660 microns. This error provides a limiting value for the roundness error of the cylindrical components using the spindle.

The aperiodic components of circle centre data are analysed for evaluating the asynchronous radial error of the spindle; it is shown in Fig. 15d. The asynchronous error of the spindle includes the contribution from structural motion of the machine structure and it is found to be non-repeatable for every revolution. It is evaluated as the maximum deviation of aperiodic components and it is found to be 85.521 microns. This error value provides the baseline value for the surface finish of the components using the spindle.

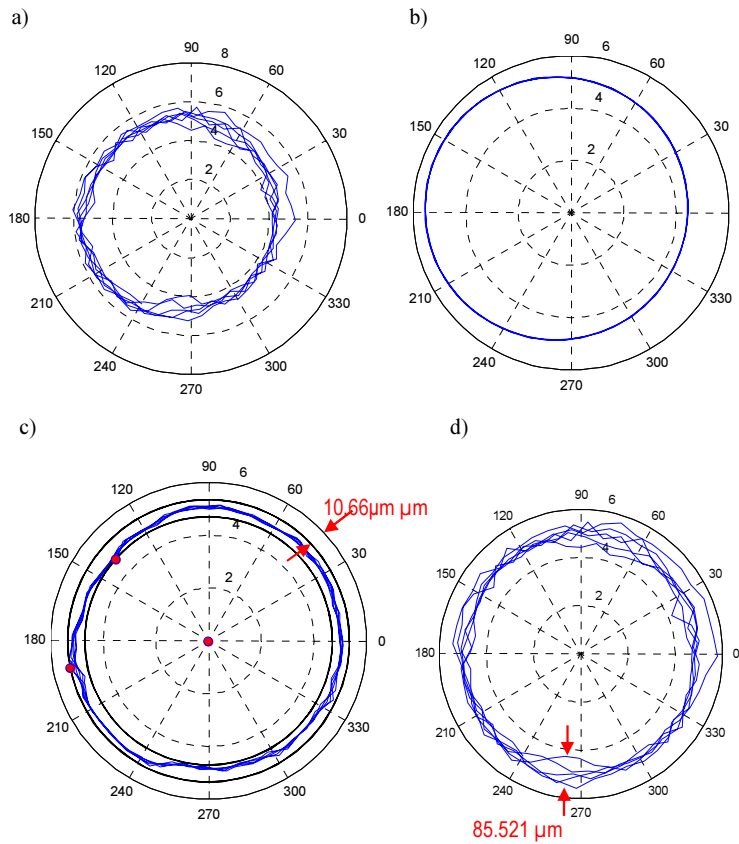


Fig. 15. Separation of the centring error and the spindle radial error for a spindle speed of 25 rpm. Coordinates of circle centre in X direction (a); centring error (b); the synchronous radial error (c); the asynchronous radial error (d).

The estimated values of synchronous and asynchronous radial errors provide a limiting value for the roundness error and surface finish of the components using the spindle. It can be noticed that the synchronous radial error is found to be decreasing with the increase in spindle speed due to a change in spindle contact during spindle rotation at the form variations in the bearing surfaces for a given spindle speed [15]. It can be noticed from Fig. 10 that the coordinates of circle centre move closer towards the average position of the master cylinder for the increase in spindle speed, hence there is a decrease in the synchronous radial error of the spindle. However, the asynchronous radial error value is found to vary randomly as it is aperiodic and also it includes the contribution from structural motion and vibration of the spindle which varies for different spindle speeds.

4.6. Repeatability of spindle radial evaluation using proposed method

In order to understand the repeatability of the spindle radial error measurements using the proposed method, the experiments have been repeated for four times and standard deviations of the estimated values were calculated and are listed in Table 5 and Table 6. It can be noticed that there is no much deviation in magnitudes of the evaluated values of synchronous and asynchronous radial errors for different experiments and they are of a similar order at various spindle speeds.

Table 5. Evaluation of the synchronous spindle radial error at different spindle speeds.

Speed (rpm)	Evaluation of Synchronous Error (μm)				Mean (μm)	Standard deviation (μm)
	Experiments					
	I	II	III	IV		
25	10.66	10.67	10.75	10.54	10.655	± 0.086603
50	13.164	13.152	13.162	13.158	13.159	± 0.005292
75	10.198	10.194	10.189	10.183	10.191	± 0.006481
100	7.542	7.538	7.541	7.537	7.5395	± 0.002380

Table 6. Evaluation of the asynchronous spindle radial error at different spindle speeds.

Speed (rpm)	Evaluation of asynchronous Error (μm)				Mean (μm)	Standard deviation (μm)
	Experiments					
	I	II	III	IV		
25	85.521	85.517	85.429	85.642	85.52725	± 0.087492
50	63.523	63.537	63.523	63.53	63.52825	± 0.006702
75	56.234	56.241	56.242	56.246	56.24075	± 0.004992
100	65.021	65.023	65.021	65.028	65.02325	± 0.003304

The maximum standard deviations of the evaluated synchronous and asynchronous radial errors are found to be $\pm 0.086603 \mu\text{m}$ and $\pm 0.087492 \mu\text{m}$, respectively. These results prove the repeatability of the proposed method for evaluation of the spindle radial error at a submicron level.

4.7. Comparison with runout estimation using dial indicator

A dial indicator is used to measure the runout of the master cylinder in a lathe, as shown in Fig. 16. The peak-to-peak variation in the dial was calculated as 150 microns for one revolution of the spindle. The proposed machine vision system provides estimation of total indicated runout of the spindle as 142 microns, as shown in Fig. 13a.



Fig. 16. Runout measurement using a dial indicator.

Since the runout estimation using a dial indicator includes the contribution from the centring error of the master cylinder, the form error of the master cylinder and the spindle radial error, its magnitude is found to be higher than the value estimated by the proposed machine vision system. That is because in the proposed method the contribution of the centring error and

the form error of the master cylinder is removed. Also, the synchronous and asynchronous radial errors are separately calculated using the curve fitting method at different spindle speeds.

5. Conclusions

Spindle radial error evaluation is an important task in understanding the machining capability of a machine tool's spindle. This paper demonstrates application of a machine vision system and a CHT-based image processing technique to evaluating the radial error of a lathe spindle at different spindle speeds. Application of CHT to detecting a circle in the image is found to be robust in estimating the circle parameters. Also, the circle detection method provides a simpler approach to eliminating the contribution of the form error of the master cylinder. In order to extract the contribution of the centring error and the radial error of the spindle, the periodic and aperiodic components of circle centre are analysed using the Fourier series curve fitting method. The synchronous radial error of a lathe spindle is found to vary between 7.542 microns and 13.164 microns for different spindle speeds and it showed a decreasing trend with the increase of the spindle speed. However, the asynchronous radial error value is found to vary randomly within a range of 56.234 microns – 85.521 microns, as it includes the contribution from structural motion of the spindle which varies for different spindle speeds. The repeatability of the spindle radial error evaluation using the proposed method is found to be at a submicron level. The proposed method can be extended to the online monitoring and estimating the spindle radial errors using a high-speed camera.

Acknowledgements

The authors wish to thank Department of Science Technology, New Delhi for providing the necessary funding to establish the machine vision system for spindle radial error measurement in machine tools under the fast track Young scientist scheme.

References

- [1] Bryan, J.B., Vanherck, P. (1975). Unification of terminology concerning the error motion of axes of rotation. *California Univ., Livermore (USA). Lawrence Livermore Lab.*
- [2] Murugarajan, A., Samuel, G.L. (2011). Measurement, modeling and evaluation of surface parameter using capacitive-sensor-based measurement system. *Metrol. Meas. Syst.*, 18(3), 403–418.
- [3] Marsh, E.R. (2008). *Precision spindle metrology*. DEStech Publications.
- [4] Liu, C.H., Jywe, W.Y., Lee, H.W. (2004). Development of a simple test device for spindle error measurement using a position sensitive detector. *Measurement science and Technology*, 15(9), 1733.
- [5] Castro, H.F. (2008). A method for evaluating spindle rotation errors of machine tools using a laser interferometer. *Measurement*, 41(5), 526–37.
- [6] Murakami, H., Kawagoishi, N., Kondo, E., Kodama, A. (2010). Optical technique to measure five-degree-of-freedom error motions for a high-speed microspindle. *International Journal of Precision Engineering and Manufacturing*, 11(6), 845–50.
- [7] Fujimaki, K., Mitsui, K. (2007). Radial error measuring device based on auto-collimation for miniature ultra-high-speed spindles. *International Journal of Machine Tools and Manufacture*, 47(11), 1677–85.
- [8] Deakyne, T.R., Marsh, E.R., Lehman, J., Bartlett, B., Solutions, C. (2008). Machine vision with spindle metrology using a ccd camera. *Proc. of ASPE 23rd Annual Meeting, American Society for Precision Engineering*, Portland.
- [9] Chen, A., Liu, N. (2010). Circular object detection with mathematical morphology and geometric properties. *IEEE, International Conference on Computer, Mechatronics, Control and Electronic Engineering*, 2, 318–321.

- [10] Jain, A.K. (1989). *Fundamentals of digital image processing*. Prentice-Hall.
- [11] Ding, L., Goshtasby, A. (2001). On the Canny edge detector. *Pattern Recognition*, 34(3), 721–725.
- [12] Smereka, M., Dulęba, I. (2008). Circular object detection using a modified Hough transform. *International Journal of Applied Mathematics and Computer Science*, 18(1), 85–91.
- [13] Shetty, P. (2011). Circle Detection in Images. *Faculty of San Diego State University*, 9–11.
- [14] Rhody, H. (2005). Lecture 10: Hough circle transform. *Chester F. Carlson Center for Imaging Science, Rochester Institute of Technology*.
- [15] Ashok, S.D., Samuel, G.L. (2012). Modeling, measurement, and evaluation of spindle radial errors in a miniaturized machine tool. *The International Journal of Advanced Manufacturing Technology*, 59(5–8), 445–61.
- [16] American National Standards Institute. (2010). ANSI / ASME Axes of Rotation: Methods for Specifying and Testing. American Society of Mechanical Engineers.
- [17] Ashok, S.D., Samuel, G.L. (2011). Least square curve fitting technique for processing time sampled high speed spindle data. *International Journal of Manufacturing Research*, 6(3), 256–276.
- [18] Ashok, S.D., Samuel, G.L. (2012). Harmonic-analysis-based method for separation of form error during evaluation of high speed spindle radial errors. *Proc. of the Institution of Mechanical Engineers, Part B: Journal of Engineering Manufacture*, 0954405411434868.